



Original Research

Multi-Factor Optimization of Adjacent Layered Salt Rock Storage Based on Response Surface Methodology

Jinyi Ji^{a,*}, Baokun Zhou^{b,**}, Zhichen Tao^{c,***}, Xiaoqing Chen^{a,****}

^a School of Mining Engineering, University of Science and Technology Liaoning, Anshan 114051, China

^b School of Energy and Mining, China University of Mining and Technology (Beijing), Beijing 100083, China

^c Anshan Iron and Steel Group Corporation, Anshan 114001, China

Received: 18 November 2022 • Accepted: 24 July 2023

ABSTRACT

In order to improve the utilization efficiency of salt rock mines when storing natural gas, it is necessary to clarify the influence of different factors on adjacent underground laminated salt rock caverns. In view of this, 15 groups of simulation tests are designed by using the Response Surface Methodology (RSM). A quadratic response surface model with the midpoint displacement and cavern waist stress of the interlayer as the response values is constructed. The influence of the interaction between pillar width, interlayer thickness and the location of a single interlayer on the midpoint displacement of the interlayer and the internal waist stress of the adjacent ellipsoidal cavity is studied. The results show that the interlayer thickness is the main influence factor of the midpoint displacement of the interlayer, and the pillar width is the main influence factor of the cavern waist stress. When the adjacent storage is designed as a pillar width of 2.5D, an interlayer thickness of 2 m, and the midpoint of the interlayer is 0.3H above the cavity, the displacement and stress of the test model are relatively small. The results can provide a certain reference for the mechanical analysis of adjacent underground layered salt rock gas storage.

Keywords: layered salt rock gas storage, multi-factor optimization, response surface methodology, finite element simulation, main influence factor

Introduction

Salt rock is an ideal oil and gas storage medium for oil and gas storage due to its low permeability and optimal creep property (Liu et al., 2016; Wanyan et al., 2019; Bakhtiari et al., 2021). Compared with the aboveground storage methods, salt rock storage has the advantages of flexible injection and production, large single-well throughput, and a high proportion of working gas (Yang, 2017; Liu et al., 2018). In addition, underground salt rock also has the characteristics of safety, saving land resources, capital and environmental protection, which is an effective way to ensure energy security (Zivar et al., 2021; Liu et al., 2020; Shad et al., 2022). The history of underground gas storage in salt rock in some countries is earlier, and the designed operation life of gas storage has been up to 80 or even hundreds of years (Patroni, 2007). China's natural gas business is developing rapidly, but the lack of gas storage capacity is still a bottleneck restricting its sustainable and high-quality development. To solve this problem, a master plan has been set to speed up the construction of underground stor-

age facilities. It will take five years to complete the total new peak capacity in the first 20 years (National Energy Administration, 2022). It is estimated that the future natural gas production will continue to grow for a long time (Lu et al., 2018). Increasing the construction of gas storage is of great significance for easing the tension between gas supply and demand in China and promoting the rapid development of economy.

To study the stability in underground salt rock storages, a geomechanical model test of Jintan underground salt rock storages was carried out to obtain the creep deformation and stress distribution of surrounding rock during the operation of gas storage (Dai et al., 2009). Jing et al. (2012) summarized the 7 factors that may affect the shrinkage deformation of salt rock storage. They presented that the operation mode of two adjacent gas storage caves (adjacent caverns or adjacent cavities for short), the ratio of low-pressure operation time in a single cycle, and the ratio of cavity height to the diameter are the main sensitive factors. Jia et al. (2014) studied the influence of geometric distribution form of el-

**** Corresponding author: xiaogchen012@126.com • <https://orcid.org/0000-0001-6714-1631>

* jild0961@163.com • <https://orcid.org/0000-0002-9277-6206>

** zhouling830@126.com • <https://orcid.org/0000-0003-0754-9226>

*** liujiangtao012@sina.com • <https://orcid.org/0000-0002-1812-2685>

lipsoidal cavity, pillar width and interlayer position on the stability of gas cavern by orthogonal experiments. Since it was proved that the interlayer position was the most significant influencing factor, the interaction between different factors and parameters cannot be effectively reflected.

Taking the underground salt rock storage in Jintan, China as the test background, reasonable test factors are selected by referring to the test parameter settings in some articles and engineering practices. 15 test plans are established by the response surface method, and the test data are obtained by establishing corresponding test models with the professional finite element simulation software. The effects of the pillar width, interlayer thickness and interlayer position on adjacent gas storage chambers are studied. Through the main effect analysis and response surface analysis of the test results, the significance and optimum level of each factor are obtained, and the optimum form of adjacent caverns during the construction of salt rock storage groups is established.

1. Parameter design of adjacent storage

The Jintan salt rock layer in Jiangsu Province is located about 1000 m deep underground with a thickness of 67.85 m to 230.95 m. The interlayer of salt rock has two layers with an average thickness of 3.02 m and 2.50 m. As of March 2023, 99 underground caverns of salt rock have been built or under construction in this salt mining area, with a single salt cavern volume of about 200,000-300,000 m³, a cavern diameter of about 70 m, a height of about 150 m, and a design pressure of about 17 MPa (Jiangsu provincial department of natural resources, 2021). The rock physical and mechanical parameters of the salt mine area are shown in Table 1 (Zhang et al., 2009). The test will use the above parameters as the basis for the gradient design of the experimental data.

Table 1: Basic parameters of strata

Formation	Elasticity modulus /GPa	Poisson ratio	Density / (kg/m ³)	Cohesion /MPa	Internal friction angle / (°)
Mudstone	10	0.27	2350	1.0	35
Interlayer	4	0.30	2350	0.5	30
Salt rock	18	0.30	2200	1.0	45

This test mainly studies the influence of different factors on the displacement and stress of sensitive parts of adjacent chambers. When simulating the initial stress of rock mass, only the gravity of rock layer is considered in the test, and Drucker-Prager model is used for numerical calculation. When simulating the initial stress of rock mass, only the static analysis of rock mass gravity is considered and the Drucker-Prager model is selected for numerical calculation. To study the influence of different factors on the stress and displacement at sensitive positions of adjacent cavities, 15 groups of corresponding three-dimensional numerical models are established to simulate the stress and displacement of adjacent cavities using the professional finite element simulation software after determining the research scheme. The calculation area is set as a cube of 800 m *800 m *400 m, and the weight of the overlying strata 700 m above the cube is simplified to the load on the top surface of the model. Based on the thickness of overburden rock and the average density of mudstone, the equivalent load above the cube is about 16 MPa. Four vertical surfaces are constrained by normal directions perpendicular to the surface. According to the actual situation of the project, the long axis of the storage cham-

ber is 150 m and its short axis is 70 m. For different test schemes, pillar width, interlayer thickness and interlayer position will vary. Figure 1 shows the cross section of the storage model with a pillar width of 105 m, an interlayer thickness of 3 m, and the interlayer midpoint is 75 m below the top of the cavern.

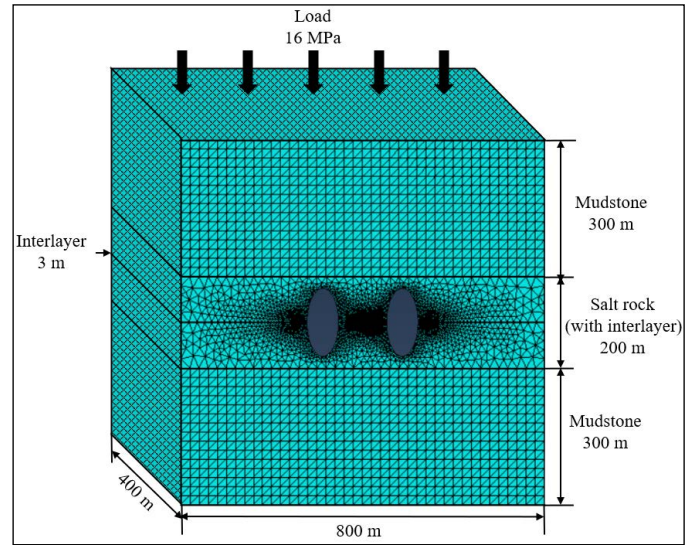


Figure 1. Cross section of the adjacent gas storage model

1.1 Design of pillar width

The overall stability of the gas storage group is closely related to the pillar width. Too narrow pillars may lead to instability and destruction of the gas storage chamber, and too wide pillars may reduce the utilization rate of salt rock mines. To prevent the destruction of gas cavern and improve the utilization efficiency of salt rock mines, a reasonable pillar width is necessary. Through the simulation of the rheology geology of the storage group with similar materials from a salt rock reservoir media model, Zhang et al. (2012) concluded that the pillar width should be greater than 1.5 times the maximum diameter of the chamber. Wang et al. (2011) used FLAC3D to establish a finite element calculation model for the simulation of saltrock gas caves. It is suggested that the width of pillars between two adjacent salt rock caves should be 2-3 times the diameter of salt cavern. Liu et al. (2011) and Jia et al. (2014) obtained an optimum pillar width 2 times the diameter of salt cave by different experimental design methods. Taking into account the above results, and to avoid waste of salt area caused by too wide pillars, the pillar width is designed to be 105 m, 140 m and 175 m, i.e. 1.5D (diameter), 2.0D and 2.5D respectively. D is the maximum diameter of the cavity waist, and 1D=70 m, as shown in Figure 2.

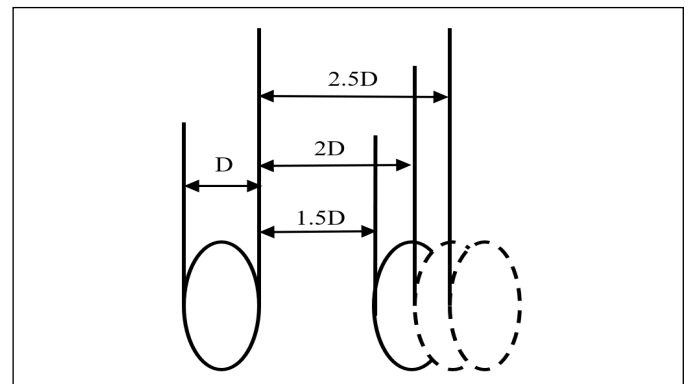


Figure 2. Design of pillar width

1.2 Design of interlayer thickness

The existence of an interlayer in a layered salt rock has an important impact on the stability of surrounding rock. Many studies show that the interlayer is usually a part of layered salt rocks prone to deformation (National Energy Administration, 2022; Lu et al., 2018). According to a creep fatigue-failure model of salt rock, Moghadam et al. (2015) found that the stability of caverns was significantly affected when the cavern surface contacted the interlayer. According to an average thickness of interlayers in a salt rock (Jiangsu provincial department of natural resources, 2021), the interlayer thickness is set as 2 m, 3 m and 4 m respectively.

1.3 Design of cavity interlayer position

According to Lu et al. (2018), the interlayer position has little influence on the stability of storage group. Jia et al. (2014) believed that there was a gap in the stress level due to different positions of the interlayer relative to the cavity. The stress level of the interlayer controls the stability of the interlayer, and then affects the stability of the cavity. It is believed that the interlayer position has a great impact on the stability of caverns. According to the results of Jia et al. (2014) and Zhang et al. (2022), the positions of the test interlayer are set as 45 m, 75 m and 105 m, i.e. $0.3H$ (height), $0.5H$ and $0.7H$ respectively. H is the maximum height of the cavity, indicating the distance between the midpoint of the interlayer and the top of the cavity in the vertical direction, and $1H=150$ m, as shown in Figure 3.

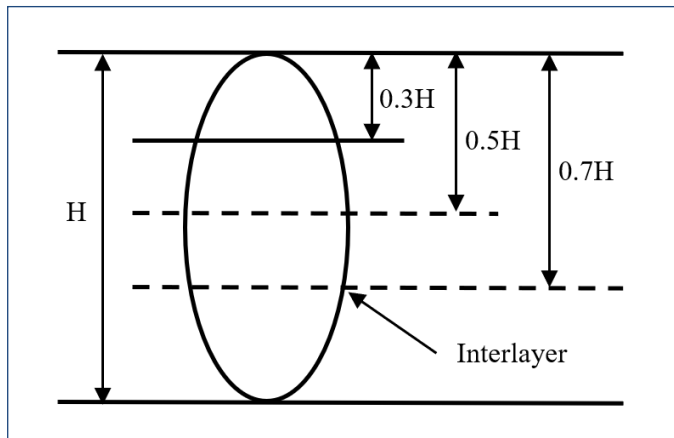


Figure 3. Design of interlayer position

2. Response surface test

2.1 Design of test scheme

Response Surface Methodology (RSM) is a statistics-based optimization method that combines the experimental design and mathematical model. It can be used to explore the mathematical relationship between multiple influencing factors and response output (Zhou et al., 2021). In this study, RSM is used to explore the influence of pillar width, interlayer thickness, interlayer position, and their interaction on the stability of adjacent cavities in the design of adjacent storages of layered salt rocks. The optimal design effect was obtained through different design tests (Chen et al., 2017). Box-Behnken Design (BBD) method was used to design the 3-factor experiment, as shown in Table 2. The code values are randomly generated by the professional data analysis software.

Table 2. Scheme design of response surface of the test factor

Test number	Code value	Pillar width(A)/m	Interlayer thickness (B)/m	Interlayer position (C)/m
1	A ₁ B ₂ C ₃	105	3	105
2	A ₁ B ₁ C ₂	105	2	75
3	A ₂ B ₂ C ₂	140	3	75
4	A ₃ B ₃ C ₂	175	4	75
5	A ₁ B ₃ C ₂	105	4	75
6	A ₂ B ₃ C ₃	140	4	105
7	A ₂ B ₃ C ₁	140	4	45
8	A ₂ B ₂ C ₂	140	3	75
9	A ₃ B ₁ C ₂	175	2	75
10	A ₃ B ₂ C ₃	175	3	105
11	A ₂ B ₁ C ₃	140	2	105
12	A ₂ B ₂ C ₂	140	3	75
13	A ₁ B ₂ C ₁	105	3	45
14	A ₃ B ₂ C ₁	175	3	45
15	A ₂ B ₁ C ₁	140	2	45

2.2 Test results and model analysis

According to the experimental scheme designed in Table 2, the corresponding finite element numerical simulation model is established, and the stress and deformation displacement of different parts of adjacent caverns are obtained when the model is loaded. As shown in Table 3, the result data of 15 groups of experiments designed by BBD and the corresponding models includes the horizontal displacement of the cavern waist and the midpoint of pillar interlayer (denoted as S and T), the equivalent stress at the midpoint of the cavern waist and the pillar interlayer (denoted as V and W), and the equivalent stress at the midpoint of the pillar and the interlayer (denoted as Y and Z). The response surface calculation function in the data analysis software is used to analyze the response surface of 6 groups of data in Table 3, and the fitting degree of different models in Table 4 is summarized. The fitting distance is measured in response variables, which represents the distance between the data value and the fitted value. The lower the fitting distance value, the higher the degree of response described by the model. The higher the R-sq (R^2) value, the higher the fitting degree between the model and the data. R-sq is always between 0% and 100%. R-sq (forecast) can be used to determine the degree to which the model can predict the response to new observations, and the model with larger R-sq (forecast) values also has better prediction.

In the correlation coefficient of the response surface function fitting of the model, the prediction R-sq by the response surface regression model for the midpoint displacement of the interlayer, the cavern waist stress, and the pillar central stress is more than 90%. It shows that the predicted data of the response surface model function is consistent with the actual data, and the error is small. It can be used to analyze and predict the effect of parameters set in the test on the adjacent caverns. Through the response results of pillar central stress, it is strongly influenced by the pillar width and can be classified as linear correlation, and is not the focus of this test. The prediction R-sq of the response surface regression model of other parameters cannot reach 90%, and no further analysis will be made.

Table 3. Regression test results of different response values

Test number	S/mm	T/mm	V/MPa	W/MPa	Y/MPa	Z/MPa
1	14.36	14.57	29.83	25.34	21.49	19.97
2	14.72	15.54	30.00	26.24	21.45	20.82
3	15.39	16.82	29.17	25.15	19.02	18.71
4	15.60	17.79	28.93	24.59	17.53	17.39
5	15.54	17.85	30.34	25.77	21.49	20.89
6	15.04	15.84	29.03	24.51	19.10	18.29
7	15.10	15.98	29.01	24.47	19.15	18.32
8	15.39	16.82	29.17	25.15	19.02	18.71
9	15.12	15.82	28.73	25.06	17.48	17.32
10	15.14	15.02	28.35	24.49	17.59	17.12
11	14.76	13.93	28.56	25.18	19.03	18.23
12	15.39	16.82	29.17	25.15	19.02	18.71
13	14.37	14.67	29.84	25.32	21.49	20.00
14	15.13	15.18	28.31	24.43	17.59	17.14
15	14.75	14.06	28.57	25.14	19.03	18.24

Table 4. Fitting degree of test models with different response values

Model summary	Fitting distance	R-sq	R-sq(ad-justment)	R-sq(forecast)
S and ABC	0.2011109	90.52%	73.45%	0.00%
T and ABC	0.136949	99.57%	98.79%	93.08%
V and ABC	0.0784538	99.43%	98.39%	90.82%
W and ABC	0.116662	98.15%	94.82%	70.42%
Y and ABC	0.0271109	99.99%	99.97%	99.81%
Z and ABC	0.203973	99.05%	97.37%	84.78%

Multivariate nonlinear quadratic fitting is performed on the interlayer midpoint displacement (*T*) and cavern waist stress (*V*) in Table 3, and the regression equations expressed in uncoded units areas (1) and (2):

$$T = -0.78 + 0.0311A + 1.293B + 0.3132C - 0.000066A^2 + 0.0112B^2 - 0.002088C^2 - 0.00243AB - 0.000014AC - 0.00008BC \quad (1)$$

$$V = 33.88 - 0.0891A + 0.183B + 0.064C + 0.000253A^2 + 0.02B^2 - 0.000442C^2 - 0.001AB + 0.000012AC + 0.00025BC \quad (2)$$

F-value and P-value are used to analyze the significance of each coefficient in the above equation. The results are shown in Table 5 and Table 6. F-value analysis is also called F-test or ANOVA (analysis of variance), which is used to evaluate the differences between groups. F-value represents the significance of the whole fitting equation. The larger the F-value, the more significant the equation and the better the fitting degree. P-value is a parameter used to determine the results of hypothesis test, which reflects the regression effect of parameters. The smaller the P-value, and the more

significant the results (Zhou et al., 2021). In addition, whether the test result is “insignificant”, “significant” or “highly significant” needs to be determined by the P-value and the actual problems. In this experiment, $P \geq 0.05$ means that the regression effect of this factor is not significant; $0.001 \leq P < 0.05$ means that the regression effect of this factor is generally significant, and $P < 0.001$ means that the regression effect of this factor is highly significant.

Table 5. Response surface regression model of interlayer midpoint displacement

Source	DoF	Adj-SS	Adj-MS	F-value	P-value	Significant
Model	9	21.5935	2.3993	127.93	<0.001	Highly significant
A	1	0.174	0.174	9.28	0.029	Significant
B	1	8.2215	8.2215	438.36	<0.001	Highly significant
C	1	0.0351	0.0351	1.87	0.23	Insignificant
AA	1	0.0244	0.0244	1.3	0.306	Insignificant
BB	1	0.0005	0.0005	0.02	0.881	Insignificant
CC	1	13.0327	13.0327	694.89	<0.001	Highly significant
AB	1	0.0289	0.0289	1.54	0.27	Insignificant
AC	1	0.0009	0.0009	0.05	0.835	Insignificant
BC	1	0	0	0	0.972	Insignificant
Error	5	0.0938	0.0188			
Loss	3	0.0938	0.0313			
Pure error	2	0	0			
Total	14	21.6873				

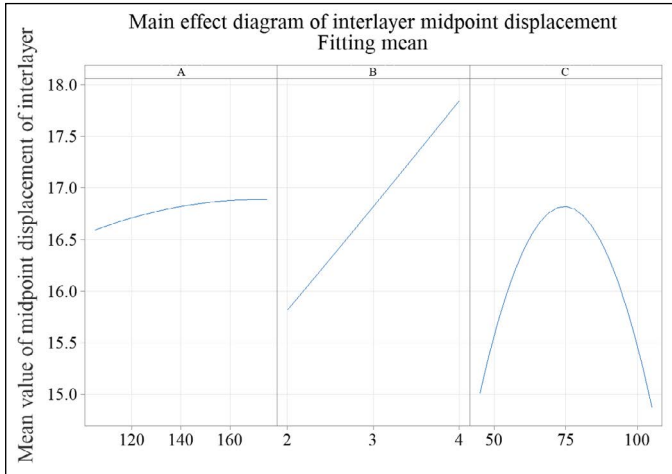
Table 6. Response surface regression model of cavern waist stress

Source	DoF	Adj-SS	Adj-MS	F-value	P-value	Significant
Model	9	5.33258	0.59251	96.26	<0.001	Highly significant
A	1	4.04701	4.04701	657.52	<0.001	Highly significant
B	1	0.26281	0.26281	42.7	0.001	Significant
C	1	0.0002	0.0002	0.03	0.864	Insignificant
AA	1	0.35483	0.35483	57.65	0.001	Significant
BB	1	0.00148	0.00148	0.24	0.645	Insignificant
CC	1	0.58341	0.58341	94.79	<0.001	Highly significant
AB	1	0.0049	0.0049	0.8	0.413	Insignificant
AC	1	0.00063	0.00063	0.1	0.763	Insignificant
BC	1	0.00023	0.00023	0.04	0.856	Insignificant
Error	5	0.03078	0.00616			
Loss	3	0.03078	0.01026			
Pure error	2	0	0			
Total	14	5.36336				

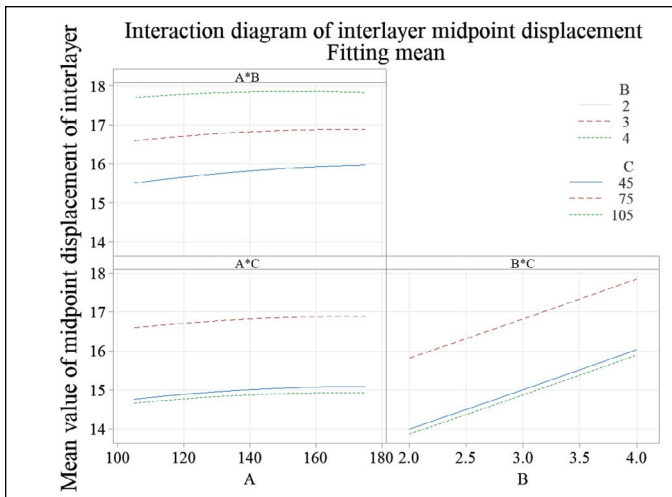
According to Table 5 and Table 6, the P-value of the interlayer midpoint displacement and the cavern waist stress response surface model are both less than 0.001, indicating that these two models are highly significant in fitting. In this model, the P-value of pillar width and interlayer thickness are both less than 0.05, indicating that they have significant effects on the midpoint displacement of the interlayer. The interlayer thickness has a highly significant effect on the midpoint displacement of interlayer, and the pillar width has a highly significant effect on the cavern waist stress.

2.3 Factor effect and response surface analysis

Based on the response surface prediction equation, the factor response diagram and response surface of the interaction between the midpoint displacement and cavern waist stress of the interlayer and the three influencing factors of the pillar width, interlayer thickness and interlayer position are shown in Figs. 4-7. The relationship between each factor and the response value can be seen intuitively in the factor response graph. In the response surface graph, the influence of the factor on the response value is reflected in the slope of the response surface. If the slope is steep, the influence of the factor is great; otherwise, it is small.

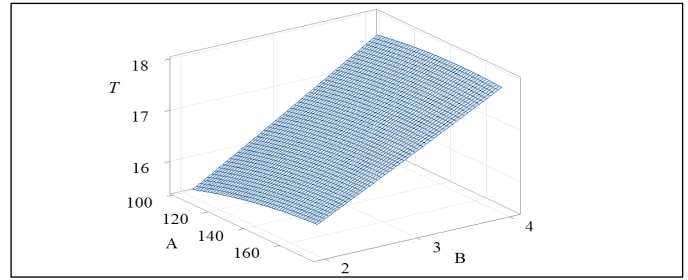


(a) Main effect diagram of interlayer midpoint displacement

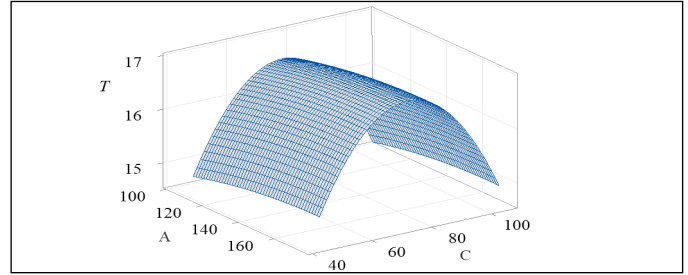


(b) Interaction diagram of interlayer midpoint displacement

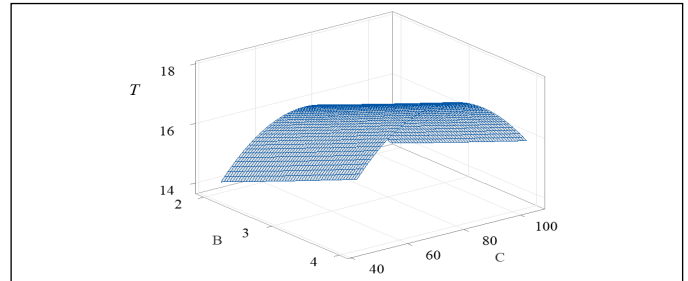
Figure 4. Factor response of interlayer midpoint displacement



(a) Effect of A*B

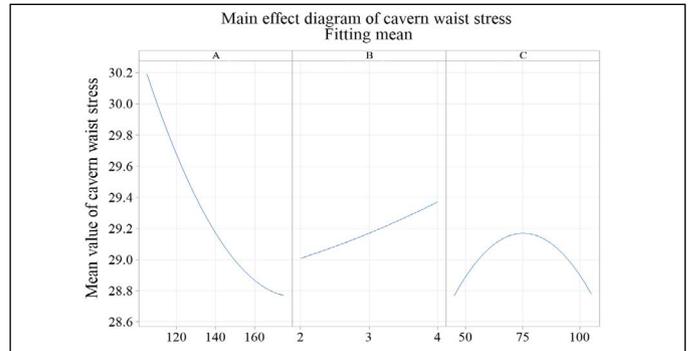


(b) Effect of A*C

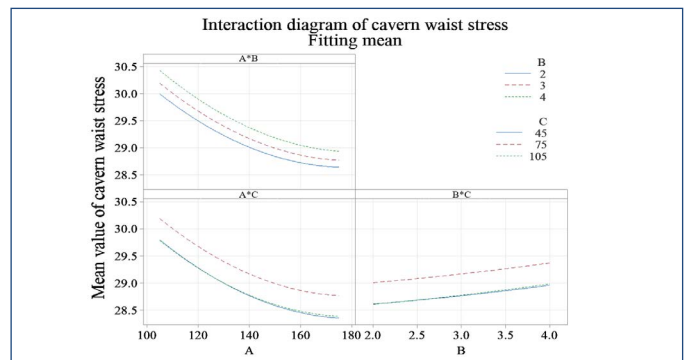


(c) Effect of B*C

Figure 5. Response surface of interlayer midpoint displacement

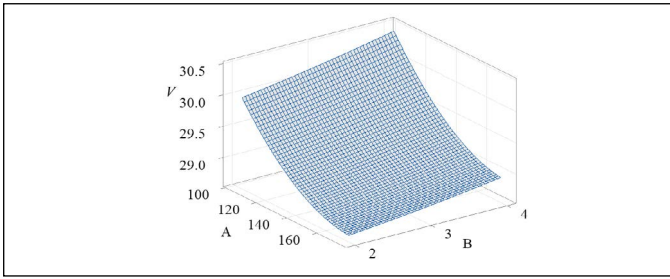


(a) Main effect diagram of cavern waist stress

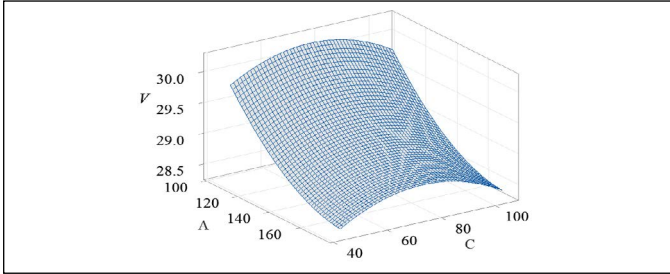


(b) Interaction diagram of cavern waist stress

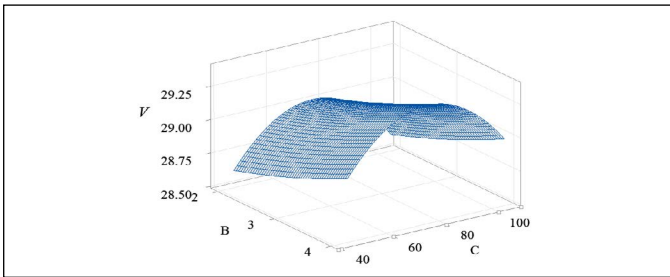
Figure 6. Factor response of cavern waist stress



(a) Effect of A*B



(b) Effect of A*C



(c) Effect of B*C

Figure 7. Response surface of cavern waist stress

It can be seen from Figure 4 and Figure 5 that the interlayer midpoint displacement increases slightly with the increase of the pillar width set in the test. Combined with the P-value of the interlayer thickness in Table 5, the displacement is mainly affected by the interlayer thickness and increases as it increases. When the interlayer is located at the waist of the cavity, the interlayer midpoint displacement is the largest and grows significantly with the increase of pillar width and interlayer thickness. It can be seen from Figure 5 (a) that the response surface is relatively steep. A and B have obvious interaction, and the displacement is more affected by the pillar width than the interlayer thickness. The optimal result is 105 m pillar width and 2 m interlayer thickness. It can be seen from Figure 5 (b) that the displacement first increases and then decreases as the interlayer depth increases, and the optimal result response is 105 m below the storage top. In Figure 5 (c), although the slope of the response surface is gentle, the range of displacement values is the largest. When the interlayer is located at the waist of the cavity, the displacement increases with the increase of the interlayer thickness.

Table 7. Multiple model response results

Response	Aim	Lower limit	Upper limit	Fitting value	SD of fitting value	Confidence interval 95%	Forecast interval 95%
S and ABC	Min	14.36	15.6	14.836	0.238	(14.225, 15.447)	(14.036, 15.636)
T and ABC	Min	13.93	17.85	14.169	0.162	(13.753, 14.585)	(13.624, 14.714)
V and ABC	Min	28.31	30.34	28.235	0.0927	(27.9967, 28.4733)	(27.9228, 28.5472)
W and ABC	Min	24.43	26.24	24.735	0.138	(24.381, 25.089)	(24.271, 25.199)
Y and ABC	Min	17.48	21.49	17.5325	0.032	(17.4502, 17.6148)	(17.4246, 17.6404)
Z and ABC	Min	17.12	20.89	16.991	0.241	(16.372, 17.611)	(16.180, 17.803)

It can be seen from Figure 6 and Figure 7 that the cavern waist stress decreases significantly with the increase of the pillar width set in the test. Based on the P-value of the pillar width in Table 6, the stress is mainly affected by the pillar width and increases with the decrease of the pillar width. When the interlayer is located at the waist of the cavity, the stress in the cavern waist is the largest and grows significantly with the increase of the interlayer thickness. It can be seen from Figure 7 (a) that the response surface is relatively steep, A and B have obvious interaction, and the stress is less affected by the interlayer thickness than the pillar width. The optimal results are 175 m pillar width and 2 m interlayer thickness. It can be seen from Figure 7 (b) that the stress first increases and then decreases with the increase of the interlayer depth, and the optimal result response is 45 m below the top of the storage. It can be seen from Figure 7 (c) that when the interlayer is located at the waist of the cavity, the stress increases with the increase of the interlayer thickness.

To determine the optimal form of adjacent caverns, 6 responses are required at least to obtain the optimal solution. In the data analysis software, the weights of 6 groups of response models are set to 1 for response, and the response results of multiple models are obtained as shown in Table 7. The optimal solution of the pillar width, interlayer thickness, and interlayer location is 175 m, 2 m and 45 m, respectively. As shown in Figure 8, a finite element model is built by the optimal solution, and the displacement and stress data at each location are obtained. The values of S, T, V, W, Y and Z are 14.92, 14.24, 28.13, 24.6, 17.54 and 17.10, respectively. Comparing the data with the fitted values and confidence intervals of the corresponding models in Table 7, it can be seen that the optimal solution model values are located in 95% confidence intervals and 95% prediction intervals. This shows that the predicted results of the multi-model response are consistent with the data obtained from the finite element model, and the error is small. To this end, the optimal solution model can be used to analyze and predict the influence of pillar width, interlayer thickness and interlayer position on the corresponding displacement and stress of adjacent caverns in Jintan.

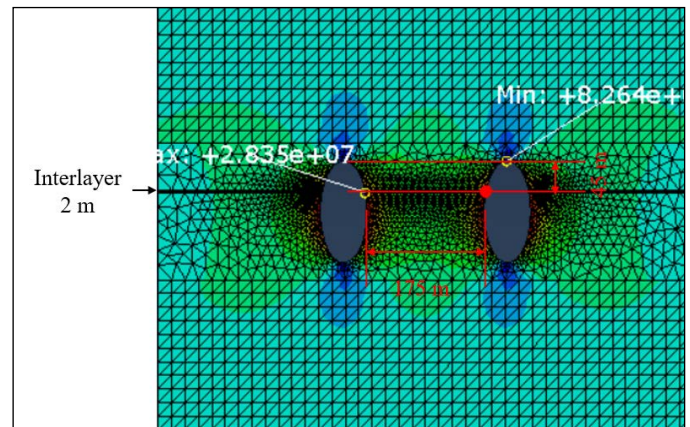


Figure 8. Finite element model of the optimal solution for each part

3. Conclusion

15 groups of simulation tests are designed using the Box-Behnken method of response surface model. The response surface model is established with the displacement of interlayer midpoint and the stress of the cavern waist as the response values. The thickness of the interlayer is the most significant factor of interlayer midpoint displacement, and the position of the interlayer follows the second. Pillar width is the most significant factor affecting the cavern waist stress, and the interlayer thickness and interlayer position are the subsignificant factors. According to the parameters set in the test, the optimal form of the adjacent storage is a pillar width of $2.5D$, an interlayer thickness of 2 m, and the midpoint of the interlayer is $0.3H$ above the cavity. Considering the stability and economy of the salt rock underground reservoir group, the column width can also be designed according to 2D.

The above static analysis conclusion can provide a model basis for the idle state of adjacent underground salt rock storage. For other projects with similar geological conditions, the proposed method can be used for modeling analysis and optimization in engineering practices.

Conflicts of interest/Competing interests

We declare that we do not have any commercial or associative interest that represents a conflict of interest in connection with the work submitted.

Availability of data and material

The datasets used or analysed during the current study are available from the corresponding author on reasonable request.

References

Bakhtiari, M., Shad, S., Zivar, D., & Razaghi, N. 2021. Coupled hydro-mechanical analysis of underground gas storage at Sarajeh field, Qom formation, Iran. *Journal of Natural Gas Science and Engineering*, 92: 103996. <https://doi.org/10.1016/j.jngse.2021.103996>

Chen, S.M., Wu, A.X., Wang, Y.M., Chen, X. 2017. Optimization research on slope structure parameters in broken rock conditions based on the response surface method. *Chinese Journal of Rock Mechanics and Engineering*, 36(S1): 3499-3508. Doi: 10.13722/j.cnki.jrme.2016.0715.

Dai, Y.H., Chen, W.Z., Yang, C.H., Tan, X.J., Jiang, X.L. 2009. A study of model test of Jintan rock salt gas storage's operation. *Rock and Soil Mechanics*, 30(12): 3574-3580. Doi: 10.16285/j.rsm.2009.12.029.

Jia, C., Zhang, K., Zhang, Q.Y., Xu, K. 2014. Research on multi-factor optimization of underground laminated salt rock storage group based on orthogonal experimental design. *Rock and Soil Mechanics*, 35(6): 1718-1726. Doi: 10.16285/j.rsm.2014.06.015.

Jiangsu provincial department of natural resources, 2021. Jintan, Changzhou "Using salt caves as storage". <http://zrzy.jiangsu.gov.cn/xwzx/ztcj/d52gsjdqr/jyiylyzy/2021/04/16101925960788.html>.

Jing, W.J., Yang, C.H., Li, L.M., Yuan, Z.Y., Shi, X.L., Li, Y.P. 2012. Sensitivity analysis of influence factors of cavity shrinkage risk in salt cavern gas storage. *Chinese Journal of Rock Mechanics and Engineering*, 31(9): 1804-1812.

Liu, J., Song, J., Zhang, Q.Y., Zhang, W.Q., Jia, C., Li, S.C., Yang, C.H. 2011. Numerical calculation and analysis of distance among salt rock underground gas storage caverns. *Chinese Journal of Rock Mechanics and Engineering*, 30(S2): 3413-3420.

Liu, W., Jiang, D., Chen, J., Daemen, J. J. K., Tang, K., & Wu, F. 2018. Comprehensive feasibility study of two-well-horizontal caverns for natural gas storage in thinly-bedded salt rocks in China. *Energy*, 143: 1006-1019. <https://doi.org/10.1016/j.energy.2017.10.126>

Liu, W., Muhammad, N., Chen, J., Spiers, C. J., Peach, C. J., Deyi, J., & Li, Y. 2016. Investigation on the permeability characteristics of bedded salt rocks and the tightness of natural gas caverns in such formations. *Journal of Natural Gas Science and Engineering*, 35(Part. A):468-482. <https://doi.org/10.1016/j.jngse.2016.07.072>

Liu, W., Zhang, Z., Chen, J., Jiang, D., Wu, F., Fan, J., & Li, Y. 2020. Feasibility evaluation of large-scale underground hydrogen storage in bedded salt rocks of China: A case study in Jiangsu province. *Energy*, 198: 117348. <https://doi.org/10.1016/j.energy.2020.117348>

Lu, J.L., Zhao, S.P., Sun, Y.P., Tang, H.J. 2018. Natural gas production peaks in China: Research and strategic proposals. *Natural Gas Industry*, 38(1): 1-9.

Moghadam, S. N., Nazokkar, K., Chalaturnyk, R. J., & Mirzabozorg, H. 2015. Parametric assessment of salt cavern performance using a creep model describing dilatancy and failure. *International Journal of Rock Mechanics and Mining Sciences*, 79: 250-267. <https://doi.org/10.1016/j.ijrmm.2015.06.012>

National Energy Administration, 2022. China's gas storage construction achieves original technical breakthrough. http://www.nea.gov.cn/2022-03/21/c_1310523065.htm.

Patroni, J. M. 2007. Life time of a natural gas storage well assessment of well-field maintenance cost. *Oil and Gas Science and Technology*, 62(3): 297-309. <https://doi.org/10.2516/ogst:2007025>

Shad, S., Razaghi, N., Zivar, D., & Mellat, S. 2022. Mechanical behavior of salt rocks: Geomechanical model. *Petroleum*. <https://doi.org/10.1016/j.petlm.2022.09.002>

Wang, T. T., Yan, X. Z., Yang, H. L., & Yang, X. J. 2011. Stability analysis of pillars between bedded salt cavern gas storages. *Journal of China Coal Society*, 36(5): 790-795.

Wanyan, Q., Xiao, Y., & Tang, N. 2019. Numerical simulation and experimental study on dissolving characteristics of layered salt rocks. *Chinese Journal of Chemical Engineering*, 27(5): 1030-1036. <https://doi.org/10.1016/j.cjche.2019.01.004>

Yang H.J. 2017. Construction key technologies and challenges of salt-cavern gas storage in China. *Oil & Gas Storage and Transportation*, 36(7): 747-753.

Zhang, H.B., Gao, K., Gou, Y.X., Ran, L.N., Li, K. 2022. Study on influence of interlayer on stability of injection-production operation of salt rock gas storage. *Journal of Safety Science and Technology*, 18(1): 29-35.

Zhang, Q.Y., Duan, K., Xiang, W., Yang, C.H., Cai, B., Xu, X.B., Jia, C., Liu, J. 2012. Three-dimensional rheological model test study of operational stability of deep laminated salt rock gas storage group under influence of extreme risk factors. *Chinese Journal of Rock Mechanics and Engineering*, 31(9): 1766-1775.

Zhang, Q.Y., Liu, D.J., Jia, C., Shen, X., Liu, J., Duan, K. 2009. Development of geomechanical model similitude material. *Rock and Soil Mechanics*, 30(12): 3581-3586. Doi: 10.16285/j.rsm.2009.12.002.

Zhou, B.K., Chen, X.Q., Tian, Y.C., Ma, D., Gong, G.H., Zhai, X.D., Deng, H.Z. 2021. Optimization of Slope Structure Parameters by Caving Method Based on Response Surface Method. *Metal Mine*, (3): 67-73. Doi: 10.19614/j.cnki.jsks.202103010.

Zivar, D., Kumar, S., & Foroozesh, J. 2021. Underground hydrogen storage: A comprehensive review. *International Journal of Hydrogen Energy*, 46(45): 23436-23462. <https://doi.org/10.1016/j.ijhydene.2020.08.138>

